AGU PUBLICATIONS

JGR

Journal of Geophysical Research: Atmospheres

RESEARCH ARTICLE

10.1002/2016JD025467

Key Points:
- The first nationwide measurements of BSOA tracers showed high concentrations in southern China
- Unexpected increases of SOA from monoterpenes and β-caryophyllene during winter were correlated with biomass burning
- BSOC composition dramatically changed from a monoterpene majority in fall-spring to an isoprene majority in summer

Supporting Information:
- Supporting Information S1
- Data Set S1
- Data Set S2

Correspondence to:
X. Ding,
xiangd@gig.ac.cn

Citation:
Ding, X., et al. (2016), Spatial and seasonal variations of secondary organic aerosol from terpenoids over China, *J. Geophys. Res. Atmos.*, *121*, 14,661–14,678, doi:10.1002/2016JD025467.

Received 6 JUN 2016
Accepted 28 NOV 2016
Accepted article online 9 DEC 2016
Published online 22 DEC 2016

Spatial and seasonal variations of secondary organic aerosol from terpenoids over China

Xiang Ding[1], Yu-Qing Zhang[1], Quan-Fu He[1], Qing-Qing Yu[1], Ru-Qin Shen[1], Yanli Zhang[1], Zhou Zhang[1], Su-Jun Lyu[1], Qi-Hou Hu[1], Yue-Si Wang[2], Long-Feng Li[3], Wei Song[1], and Xin-Ming Wang[1]

[1]State Key Laboratory of Organic Geochemistry and Guangdong Provincial Key Laboratory of Environmental Protection and Resources Utilization, Guangzhou Institute of Geochemistry, Chinese Academy of Sciences, Guangzhou, China, [2]State Key Laboratory of Atmospheric Boundary Layer Physics and Atmospheric Chemistry, Institute of Atmospheric Physics, Chinese Academy of Sciences, Beijing, China, [3]School of Chemistry and Material Sciences, Huaibei Normal University, Huaibei, China

Abstract A majority of global secondary organic aerosol (SOA) comes from terpenoids. In this study, we carried out a 1 year nationwide observation of pinenes (α- and β-pinene) and SOA tracers from monoterpenes (SOA_M) and β-caryophyllene (SOA_C) over China for the first time. SOA_M and SOA_C tracers ranged from 9.80 to 49.0 ng m^{-3} and 1.72 to 7.72 ng m^{-3}, respectively, with high levels in southern China. Pinenes ranged from 34 to 102 parts per trillion by volume, with α-pinene dominant over β-pinene. SOA_M tracers were correlated between paired sites, suggesting a regional impact of SOA_M, while pinenes were uncorrelated between sites due to their rapid oxidation. High levels of SOA_M tracers were observed in spring and summer. However, at the Hailun site in Northeast China, SOA_M tracers increased during winter. The positive correlation between SOA_M tracers and the biomass burning (BB) tracer levoglucosan during winter at Hailun indicated that the unexpected increase of SOA_M was associated with BB. The SOA_C tracer, β-caryophyllenic acid, increased during winter and was positively correlated with levoglucosan, suggesting substantial contributions from BB to SOA_C production in wintertime. Together with SOA tracers from isoprene, these tracers were applied to estimate biogenic secondary organic carbon (BSOC) from isoprene, monoterpenes, and β-caryophyllene. The annual average BSOC was 0.91 ± 0.41 μgC m^{-3},with the majority from monoterpenes and the highest level in Southwest China. BSOC was elevated from April to September and was lowest in January and February. BSOC composition dramatically changed from a monoterpene majority in fall-spring to an isoprene majority in summer.

1. Introduction

Organic aerosol (OA) affects the Earth's radiation balance, regional air quality, and public health. As a major contributor to the global OA budget, secondary organic aerosol (SOA) is produced by the reactions of volatile organic compounds (VOCs) with ozone (O_3), hydroxyl (OH), and nitrate (NO_3) radicals and is formed through condensation on and/or uptake by preexisting particles. On a global scale, annual emissions of biogenic VOCs (BVOCs) have been estimated to be 760 TgC yr^{-1}, consisting of 70% isoprene, 11% monoterpenes, and 2.5% sesquiterpenes [*Sindelarova et al.*, 2014], while the emissions of anthropogenic VOCs (AVOCs) are only ~130 Tg yr^{-1}, as derived from Global Emissions InitiAtive (http://geiacenter.org). Considering the difference in SOA yields between BVOCs and AVOCs, models predict that global SOA mostly originates from BVOCs [*Hallquist et al.*, 2009].

Due to limited knowledge about BVOC emissions and biogenic SOA (BSOA) formation mechanisms, simulation results exhibit large model-to-model differences. For instance, some global SOA models predicted the dominance of isoprene (SOA_I) over monoterpenes (SOA_M) [*Heald et al.*, 2008; *Lin et al.*, 2016], while some showed the dominance of SOA_M over SOA_I [*Farina et al.*, 2010; *Pye et al.*, 2010]. Such a discrepancy in simulation results is also documented in regional models, e.g., in China [*Fu et al.*, 2012; *Han et al.*, 2008].

Large-scale and long-term field observations can provide important information on SOA amount, composition, and spatiotemporal distribution, which is vital to constrain models. From regional to global scales, ambient levels of SOA or secondary organic carbon (SOC) have been estimated based on measurements of organic carbon (OC) and elemental carbon [*Hand et al.*, 2011; *Xin et al.*, 2014], water-soluble OC

[*de Gouw et al.*, 2008; *Ding et al.*, 2008], SOA tracers [*Ding et al.*, 2013; *Fu et al.*, 2011], and oxygenated OA by aerosol mass spectrometry [*Zhang et al.*, 2007].

SOA tracers can provide insight into SOA formation and evolution mechanisms. For instance, SOA_M formation undergoes multiple reactions. *cis*-Pinonic acid (PNA) and pinic acid (PA) are the first-generation SOA_M products from both O_3 and OH oxidation of α-pinene [*Eddingsaas et al.*, 2012; *Jenkin et al.*, 2000]. PNA and PA can be further photodegraded to high-generation products, e.g., 3-methyl-1,2,3-butanetricarboxylic acid (MBTCA) [*Claeys et al.*, 2007; *Müller et al.*, 2012; *Szmigielski et al.*, 2007]. The ratio of PNA plus PA to MBTCA has been applied to trace the aging of SOA_M [*Ding et al.*, 2011; *Gómez-González et al.*, 2012]. Recently, *Zhang et al.* [2015a] explicitly identified the molecular products of monomers and dimers in SOA_M and discovered an additional particle-phase pathway for PA production through diacyl peroxide decomposition. In addition, the ratio of 3-hydroxyglutaric acid (HGA) to MBTCA in SOA_M can be used to distinguish α-pinene from other monoterpenes [*Lewandowski et al.*, 2013], although the photo-oxidation of other monoterpenes, such as δ-limonene and β-pinene, has identical or isobaric products to α-pinene [*Jaoui et al.*, 2005].

As the largest developing country, China is suffering from a serious particulate matter (PM) problem [*Guo et al.*, 2014; *Zhang et al.*, 2012a]. During extremely severe haze pollution events in China, organic matter (OM) constitutes a major fraction (30–50%) of $PM_{2.5}$ (PM with an aerodynamic diameter less than 2.5 μm), and SOA contributes up to 70% of OM [*Huang et al.*, 2014]. Thus, SOA plays an important role in PM pollution in China. Previous modeling studies showed that SOA was mainly from BVOCs in China, although the relative abundances of SOA_I and SOA_M varied from model to model [*Fu et al.*, 2012; *Han et al.*, 2008; *Jiang et al.*, 2012]. Our ground-based observation during summer in the six regions of China illustrated that isoprene was the major precursor of BSOA [*Ding et al.*, 2014]. The annual average SOC from isoprene (SOC_I) ranged from 0.03 to 0.63 μgC m^{-3} over China, and SOC_I levels increased in summertime and significantly decreased during fall to spring [*Ding et al.*, 2016]. At present, nationwide observation of BSOA from monoterpenes and sesquiterpenes is rare in China. In this study, we focused on SOA tracers from monoterpenes and β-caryophyllene at 12 sites in China and characterized their spatial and seasonal trends. α-Pinene and β-pinene were also analyzed at 6 of the 12 sites to determine the relationship between SOA_M tracers and their precursors. In addition, SOC from monoterpenes (SOC_M) and β-caryophyllene (SOC_C) were estimated by using the SOA-tracer method and were compared with the previously reported SOC_I [*Ding et al.*, 2016] to illuminate spatial and seasonal variations of biogenic SOC (BSOC) amount and composition over China.

2. Experimental Section

2.1. Field Sampling

Particle samples were simultaneously collected at 12 sites across six regions of China, including five urban sites, three suburban sites, and four rural sites (Figure S1 in the supporting information). The 12 sites cover seven temperate zones in China with diverse vegetation types (Table S1 in the supporting information). Total suspended particles were collected by using Anderson nine-stage cascade impactors equipped with quartz fiber filters (Whatman, prebaked at 450°C for 8 h) at an airflow rate of 28.3 L/min. The 50% cutoff sizes were $<$0.4, 0.4–0.7, 0.7–1.1, 1.1–2.1, 2.1–3.3, 3.3–4.7, 4.7–5.8, 5.8–9.0, and $\geq$9.0 μm. One set of nine size-fractionated filters was collected for 48 h every 2 weeks at each site. In this study, 294 sets of particle samples were collected from October 2012 to September 2013. Additionally, one set of field blanks was collected at each site in the same way as ambient samples for 5 min when the sampler was turned off. The SOA study is a subproject of a national aerosol campaign that primarily aims to determine the size distribution of major components in PM over China [*Xin et al.*, 2014].

VOC samples were simultaneously collected at 6 of the 12 sites (Table S1) every Wednesday at approximately 14:00 local time. Ambient air was compressed into a cleaned and evacuated 1 L silonite-treated stainless steel canister (Entech Instruments Inc.) to ~2×10^5 Pa in approximately 1 h by an oil-free pump. A total of 270 VOC samples were collected from October 2012 to September 2013.

2.2. Chemical Analysis

Since not all size-fractionated filters had detectable levels of these SOA tracers, to compare tracer levels at the 12 sites for the whole year, we combined each set of nine filters into one sample for chemical analysis. Detailed information on SOA tracer analysis is described elsewhere [*Ding et al.*, 2014; *Shen et al.*, 2015].

Prior to solvent extraction, deuterated dodecanoic acid (dodecanoic acid-d_{23}) was spiked into the samples as the internal standard for SOA_M and SOA_C tracer quantification. Samples were extracted twice by sonication with the mixed solvent dichloromethane (DCM)/hexane (1:1, vol/vol), followed by 3 times with the mixed solvent of DCM/methanol (1:1, vol/vol). The extracts of each sample were combined, filtered, and concentrated to ~2 mL. Then, the concentrated solution was divided into two parts for methylation and silylation, respectively.

The derivatized samples were analyzed with an Agilent 7890/5975C gas chromatography/mass spectrometer detector (GC/MSD) in the selected ion monitoring (SIM) mode with a 30 m HP-5 MS capillary column (i.d. 0.25 mm, 0.25 μm film thickness). Splitless injection of a 2 μL sample was performed. The GC temperature was initiated at 65°C (held for 2 min) and increased to 290°C at 5°C min^{-1} and held for 20 min. In this study, six SOA tracers were quantified by GC/MSD coupled with an electron impact (EI) ionization source, including five SOA_M tracers: PNA, PA, MBTCA, HGA, and 3-hydroxy-4,4-dimethylglutaric acid (HDMGA), as well as one SOA_C tracer: β-caryophyllenic acid (CA). PNA and PA were quantified by using authentic standards. Due to the lack of commercial standards, the other SOA_M tracers were quantified by using PNA and CA was quantified by using octadecanoic acid [*Ding et al.*, 2011, 2012]. Data Set S1 in the supporting information lists all the measurements of these SOA tracers at the 12 sites in China. It should be pointed out that the SOA tracers reported in this study do not cover all BVOCs (e.g., sesquiterpenes other than β-caryophyllene and other monoterpenes) and that what is called the SOA_M tracer is somewhere in between a tracer for α-pinene and a tracer for a somewhat broader group of monoterpenes.

VOC samples were analyzed with an Entech 7100 Preconcentrator coupled with an Agilent 5973 N gas chromatography-mass selective detector/flame ionization detector (GC-MSD/FID). The detailed three-stage preconcentration processes are described elsewhere [*Zhang et al.*, 2012b, 2015b]. Briefly, 500 mL of air samples were drawn through a liquid-nitrogen cryogenic trap with glass beads at −160°C. Then, the primary trap was heated to 10°C, and the VOCs were transferred by pure helium to the secondary trap at −50°C, with Tenax-TA as an adsorbent. Water and carbon dioxide were removed through this purge-and-trap step. Then, the secondary trap was heated to transfer the VOCs by pure helium to the third cryo-focus trap at −170°C.

After the focusing step, the trap was rapidly heated, and the VOCs were transferred to the GC-MSD/FID system. The mixture was first separated by a DB-1 capillary column (60 m × 0.32 mm × 1.0 μm) and was then split into two directions by a splitter: a 0.35 m × 0.10 mm i.d. stainless steel line connected to an MSD and an HP PLOT-Q column (30 m × 0.32 mm × 20 μm) connected to an FID. The GC temperature was initiated at 10°C (held for 3 min), increased to 120°C at 5°C min^{-1}, and increased again to 250°C at 10°C min^{-1} (held for 20 min). α-Pinene and β-pinene were identified based on their retention times and mass spectra in the MSD and were quantified by external calibration by using authentic standards. The MSD was in the SIM mode with an EI ionization source. Data Set S2 lists all the measurements of α-pinene and β-pinene at the six sites in China.

Daily average temperature, relative humidity, and the maximum solar radiation during each sampling episode were downloaded from the China Meteorological Data Sharing Service System (http://cdc.nmic.cn/home.do).

2.3. Quality Assurance and Quality Control

Field and laboratory blanks were analyzed in the same manner as the filter samples. The SOA tracers were not detected in the field or laboratory blanks. Six spiked samples (authentic standards spiked into solvent with prebaked quartz filters) were analyzed to evaluate the recovery of the analytical method. The recoveries were 101 ± 3% for PNA, 70 ± 10% for PA, and 83 ± 7% for octadecanoic acid. The relative differences for target compounds in samples collected in parallel ($n = 6$) were all less than 15%. The method detection limits (MDLs) for PNA, PA, and octadecanoic acid were 0.05, 0.07, and 0.05 ng m^{-3}, respectively, with a total volume of 81.5 m^3. Considering the errors in the field blank, recovery, and surrogate quantification, the uncertainties in the tracer analyses were 3% for PNA, 30% for PA, 60% for MBTCA, 65% for HDMGA, 95% for HGA, and 156% for CA [*Shen et al.*, 2015]. The analysis uncertainty of the sum of five SOA_M tracers was, on average, 22% through error propagation. Ketopinic acid was used as the surrogate for the quantification of all SOA tracers by *Kleindienst et al.* [2007], while different surrogates were used to quantify different SOA tracers in this study.

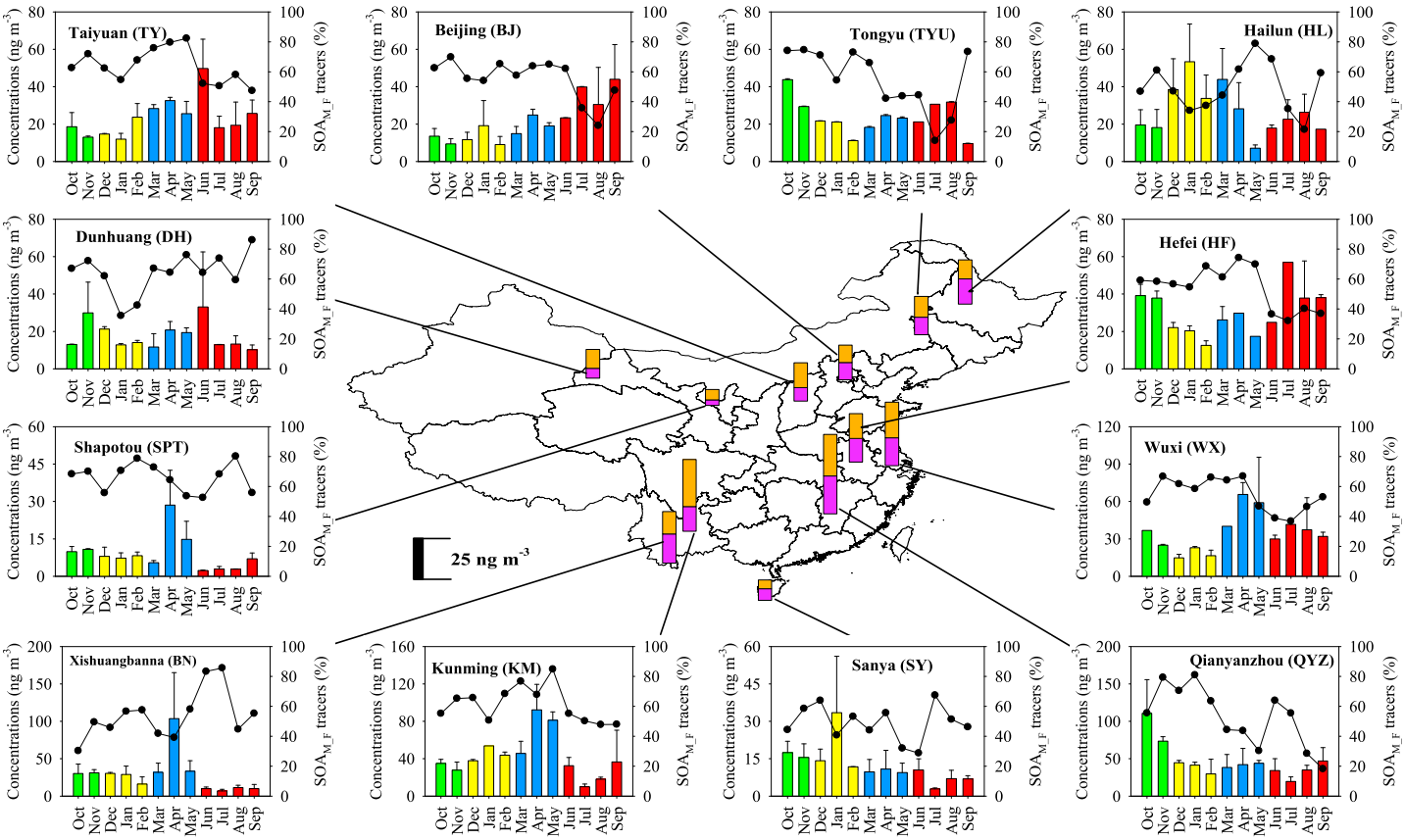

Figure 1. Spatial and seasonal variations of SOA_M tracers at 12 sites in China, including five urban sites: Beijing (BJ), Taiyuan (TY), Hefei (HF), Kunming (KM), and Dunhuang (DH); three suburban sites: Hailun (HL), Wuxi (WX), and Sanya (SY); and four rural sites: Tongyu (TYU), Shapotou (SPT), Qianyanzhou (QYZ), and Xishuangbanna (BN). The orange and magenta bars in the central figure represent the annual average of first- and high-generation products, respectively. The green, yellow, blue, and red bars represent the sum of all SOA_M tracers in fall (October–November 2012), winter (December 2012 to February 2013), spring (March–May 2013), and summer (June–September 2013), respectively. The black circle indicates the mass fraction of first-generation products in total SOA_M tracers (%).

The response factors of the internal standard calibration were 1.17 for octadecanoic acid, 1.40 for PNA, and 1.78 for PA. We also calculated the response factor of ketopinic acid (1.27), which was consistent with those of the other surrogates.

For VOCs, the canisters were cleaned at least 5 times by repeatedly filling them with pure nitrogen and evacuating before sampling. To check for potential contamination in the canisters, the vacuumed canisters after the cleaning procedure were re-filled with humidified zero air and stored in the laboratory for at least 24 h. These canisters were analyzed in the same way as field samples to ensure that the target VOCs were not present. The analytical system was tested daily with a standard mixture (~1 ppbv) before running air samples. If the response was more than ±10% of the initial calibration curve, recalibration was performed. The MDLs for α-pinene and β-pinene were both 6 parts per trillion by volume (pptv).

3. Results and Discussion

3.1. Spatial Distribution of SOA Tracers and Pinenes

The sum of SOA_M tracers ranged from 9.80 to 49.0 ng m^{-3} among the 12 sites. Our measurements were consistent with those reported in different regions of China (Table S2) [*Ding et al.*, 2012; *Feng et al.*, 2013; *Fu et al.*, 2014; *Guo et al.*, 2012; *Hu et al.*, 2008; *Li et al.*, 2013]. The highest concentration was observed at the rural Qianyanzhou (QYZ) site in East China, and the lowest level occurred at the desert Shapotou (SPT) site in Northwest China (Figure 1). East China (Wuxi (WX), Hefei (HF), and QYZ) exhibited the highest concentrations among the six regions, followed by Southwest China (Xishuangbanna (BN) and Kunming (KM)) and Northeast China (Hailun (HL) and Tongyu (TYU)). These three regions are hot spots of monoterpene emissions in China,

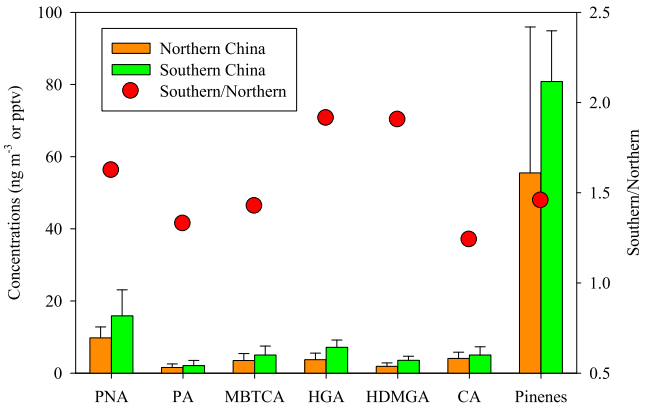

Figure 2. Comparison of tracers and pinenes in northern China (Northeast China, North China, and Northwest China) and southern China (East China, Southwest China, and South China). The red circles indicate the ratios of southern to northern regions for tracers and pinenes. The error bar means one standard deviation of each species.

as predicted by BVOC emission models that consider the land cover in China and the impacts of temperature and radiation [*Fu and Liao*, 2014; *Li and Xie*, 2014; *Tie et al.*, 2006]. North China (Beijing (BJ) and Taiyuan (TY)), Northwest China (Dunhuang (DH) and SPT), and South China (Sanya (SY)) presented relatively lower levels. The levels of all SOA_M tracers were higher in southern China than northern China ($p < 0.05$; Figure 2).

The annual average of pinenes (sum of α-pinene and β-pinene) ranged from 34 to 102 pptv among the six sites (Figure 3). α-Pinene was dominant over β-pinene, with the ratio of α-pinene to β-pinene within the range of 1.09–4.76. Previous measurements in China showed that the levels of pinenes were within the range of 30–180 pptv, with α-pinene dominant over β-pinene [*Song et al.*, 2007; *Tang et al.*, 2009; *Wang et al.*, 2013]. Our measurements are consistent with those reported in previous studies. The highest level of pinenes was observed at the rural TYU site in Northeast China, and the lowest level occurred at the desert DH site in Northwest China. Spatial differences across the northern and southern parts of China were not statistically significant for pinenes ($p > 0.05$; Figure 2).

Among the six sites where both SOA_M tracers and pinenes were measured, the spatial distribution of SOA_M tracers was different from that of pinenes. For instance, the highest annual average of SOA_M tracers occurred at KM in Southwest China, while the highest annual average of pinenes was observed at TYU in Northeast China. Within Northeast China, the HL site showed higher concentrations of SOA_M tracers but lower levels of pinenes compared with the TYU site. Ambient abundances of pinenes depend on emissions, gas-phase reactions, and meteorological conditions. Besides these factors, SOA_M formation is deeply influenced by gas-particle partitioning [*Saleh et al.*, 2013; *Sheehan and Bowman*, 2001], heterogeneous reactions [*Lal et al.*, 2012], and condensed-phase processes [*Epstein et al.*, 2014]. The complexity of SOA_M formation might explain the difference in spatial distribution between SOA_M tracers and pinenes. Moreover, the lifetimes of SOA_M tracers in the air are much longer than those of pinenes (Table S3). This implies that the transport distance of SOA_M tracers in the air is farther than that of pinenes. Thus, high levels of SOA_M tracers might not be observed at a location with high pinene emissions. In addition, the photo-oxidation of other monoterpenes, such as δ-limonene, also produces these tracers [*Jaoui et al.*, 2005]. If such an influence is significant, the spatial distribution of SOA_M tracers is expected to be different from that of pinenes. It should also be noted that the VOC samples were collected weekly over 1 h, whereas the particle samples were collected biweekly over 48 h. The lack of consistency in sampling might partly account for the disagreement in the spatial distribution of SOA_M tracers and pinenes.

Among the five SOA_M tracers, PNA was the major compound, with an annual average of 12.8 ± 6.16 ng m^{-3}, followed by HGA (5.44 ± 2.57 ng m^{-3}), MBTCA (4.27 ± 2.24 ng m^{-3}), HDMGA (2.73 ± 1.32 ng m^{-3}), and PA (1.82 ± 1.22 ng m^{-3}). α-Pinene ozonolysis produces two excited carbonyl-substituted Criegee intermediates, which further form PNA and PA, respectively [*Jenkin et al.*, 2000; *Ma et al.*, 2008]. The OH oxidation of α-pinene under NOx free conditions also produces PNA and PA [*Eddingsaas et al.*, 2012; *Zhang et al.*, 2015a]. Thus, PNA and PA are considered the first-generation products of SOA_M (SOA_{M_F} tracers). PNA and PA can be further photodegraded to the high-generation (SOA_{M_H}) product MBTCA [*Claeys et al.*, 2007; *Müller et al.*, 2012; *Szmigielski et al.*, 2007]. The ratio of PNA plus PA to MBTCA, (PNA + PA)/MBTCA, has been applied to trace SOA_M aging [*Ding et al.*, 2011; *Gómez-González et al.*, 2012]. In fresh chamber-produced α-pinene SOA samples, the ratios of (PNA + PA)/MBTCA were in the range of 1.51 to 3.21 under high-NOx conditions (with NO as the oxidant) [*Offenberg et al.*, 2007] and 3.94 to 5.91 under the low-NOx conditions (with H_2O_2 as the

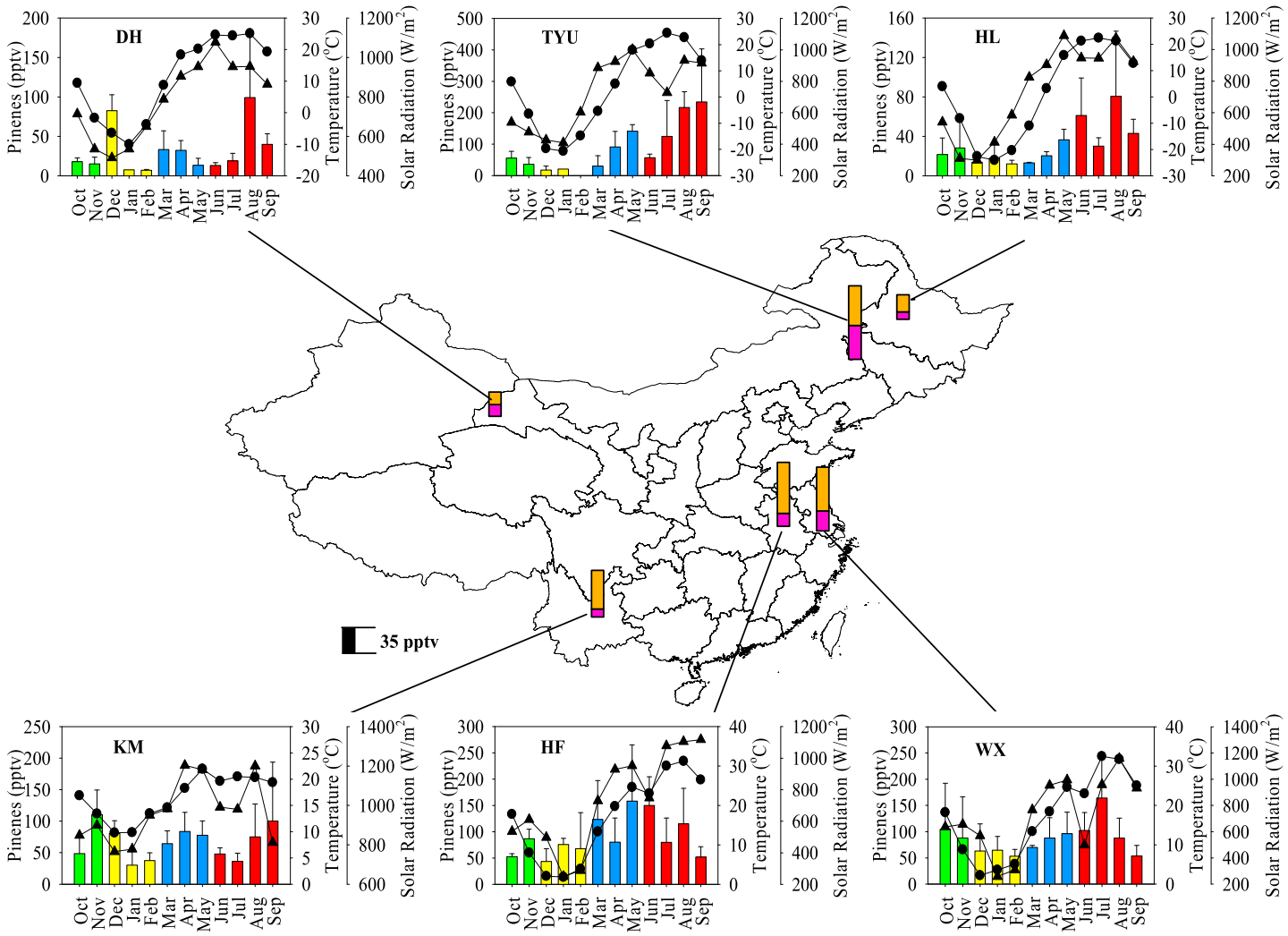

Figure 3. Spatial and seasonal variations of pinenes over China. The orange and magenta bars in the central figure represent the annual average of α-pinene and β-pinene, respectively. The green, yellow, blue, and red bars represent pinenes (sum of α-pinene and β-pinene) in fall (October–November 2012), winter (December 2012 to February 2013), spring (March–May 2013), and summer (June–September 2013), respectively. The black circle and triangle indicate temperature and solar radiation, respectively.

OH source) [*Eddingsaas et al.*, 2012]. In this study, the medians of the (PNA + PA)/MBTCA ratio varied from 2.10 (HL) to 4.81 (HF) and were within the range of fresh α-pinene SOA samples (Figure S2a). Thus, the SOA_M in China was generally SOA_{M_F}. If we regard MBCTA, HGA, and HDMGA as the SOA_{M_H} tracers [*Ding et al.*, 2014], the SOA_{M_F} tracers (sum of PNA and PA) were dominant over the SOA_{M_H} tracers (sum of HGA, HDMGA, and MBCTA) in China, with mean mass fractions of 57% in the SOA_M tracers (Figure 1).

The ratio of HGA to MBTCA (HGA/MBTCA) can be used to distinguish different monoterpenes. α-Pinene has higher yields of MBTCA compared to HGA than β-pinene or δ-limonene [*Jaoui et al.*, 2005]. *Lewandowski et al.* [2013] reported the HGA/MBTCA ratios at 15 sites across the United States. They found that the ratio was the lowest (~1.0) in the southeastern United States and the highest in California (1.83 to 3.65), indicating that α-pinene was the main precursor of SOA_M in the former. Figure S2b presents the HGA/MBTCA ratios at the 12 sites. The medians varied from 0.39 (TY) to 2.19 (SY) and were close to 1.0 at most sites, suggesting that α-pinene was the major precursor of SOA_M in China. This is in line with the conclusion that α-pinene was dominant over β-pinene in China based on their ratio.

Previous chamber studies have demonstrated that the relative abundance of PNA and PA in α-pinene SOA depends on the oxidation conditions. Under the low-NOx conditions (with H_2O_2 as the OH source), PA was

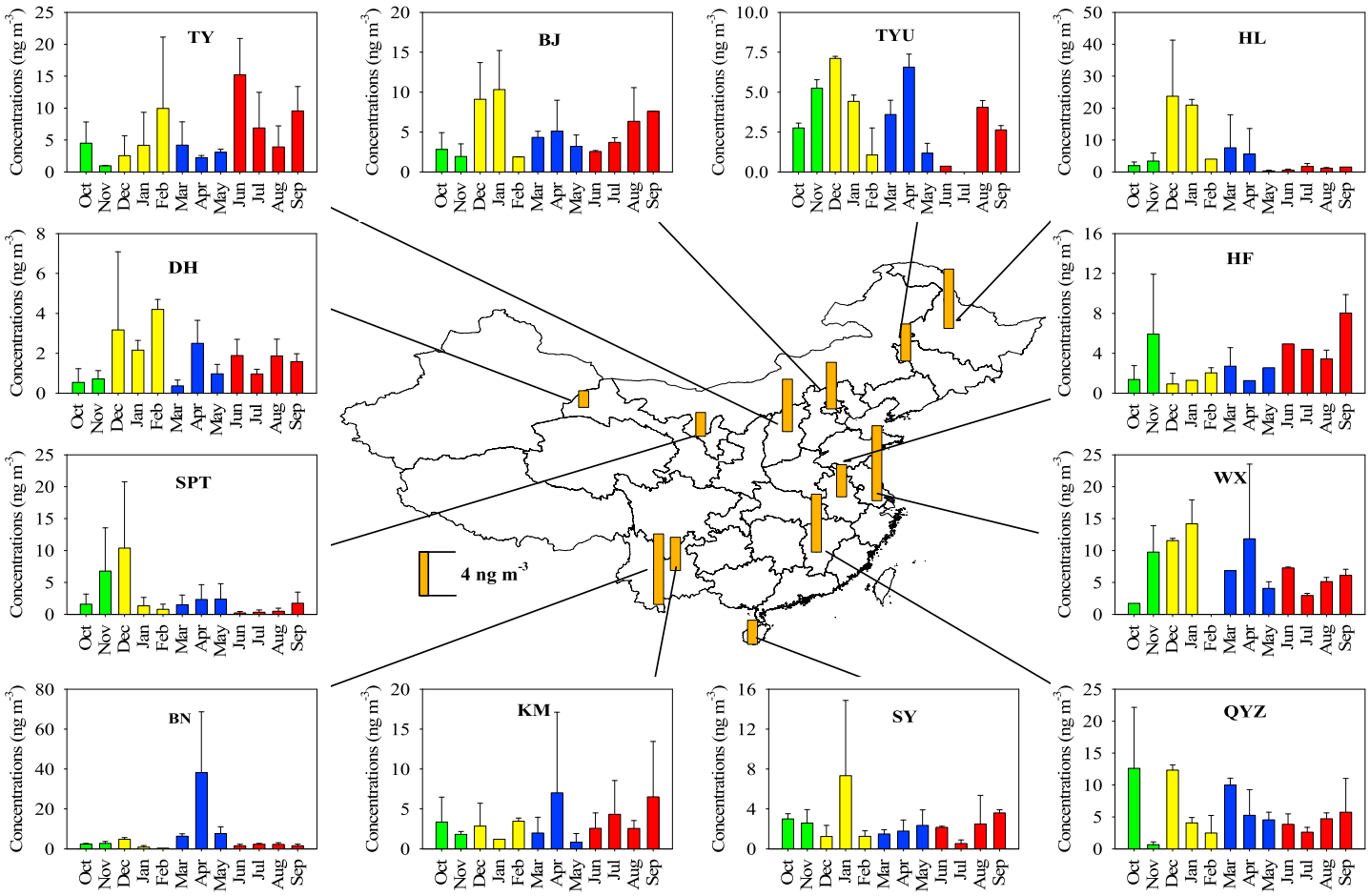

Figure 4. Spatial and seasonal variations of β-caryophyllenic acid over China. The orange bar in the central figure represents the annual average at each site. The green, yellow, blue, and red bars represent β-caryophyllenic acid in fall, winter, spring, and summer, respectively.

slightly higher than PNA, with PA/PNA ratios of 1.13–1.34 (SOA amounts of 40–77 μg m^{-3}) [*Eddingsaas et al.*, 2012]. Under the high-NOx conditions (with NO as the oxidant), PA was dominant over PNA, with PA/PNA ratios of 7.37–20.0 (SOA amounts of 113–440 μg m^{-3}) [*Offenberg et al.*, 2007]. In contrast, PNA had higher mass yield than PA in α-pinene ozonolysis [*Jenkin et al.*, 2000]. The PA/PNA ratios from α-pinene ozonolysis were reported within the range of 0.2 to 1.0, with SOA amounts less than 200 μg m^{-3} [*Presto et al.*, 2005]. *Presto et al.* [2005] found that the PA/PNA ratios increased with increasing amounts of SOA due to changes in the reaction chemistry. When chamber-produced SOA amounts exceeded 200 μg m^{-3}, PA became dominant over PNA [*Zhang et al.*, 2015a]. However, in the real atmosphere, OA amounts cannot exceed 200 μg m^{-3}, even under severe air pollution in China [*Sun et al.*, 2014]. In fact, the annual average OC at the 12 sites ranged from 22 to 54 μgC m^{-3} [*Xin et al.*, 2014], resulting in calculated OM levels within the range of 35–86 μg m^{-3} (OC × 1.6). Therefore, the ratio of PNA/PA can be applied to distinguish different α-pinene oxidation processes in ambient air. Ozonolysis has a PNA/PA ratio greater than 1.0, high-NOx NO oxidation has a PNA/PA ratio close to 1.0, and low-NOx OH oxidation has a PNA/PA ratio much less than 1.0.

In this study, the medians of the PNA/PA ratio varied from 3.10 (HL) to 20.8 (TY) and were much higher than 1.0 at all sites (Figure S2c). As discussed above, SOA_M was mainly from α-pinene in China. Thus, the observed high PNA/PA ratios indicated that ozonolysis played an important role in α-pinene oxidation in China. Because PNA and PA were not detected under the high-NO (with HONO as the OH source) and high-NO_2 (with CH_3ONO as the OH source) OH oxidation conditions [*Eddingsaas et al.*, 2012], the ratio of PNA/PA cannot be used to evaluate the importance of the whole OH oxidation pathway. Table S3 lists the rate constants and

Table 1. Correlation Coefficients Between Sites in Each Region

Region Paired Sites	East WX-HF (280 km[a])	Southwest KM-BN (380 km)	North BJ-TY (400 km)	Northeast HL-TYU (450 km)	Northwest DH-SPT (940 km)
		Meteorological Parameters			
Temperature	**0.991**[b]	**0.961**	**0.970**	**0.991**	**0.989**
Relative humidity	**0.860**	**0.732**	**0.839**	*0.448* [c]	*0.426*
Solar radiation	**0.901**	0.232	**0.815**	**0.906**	**0.671**
		Pinenes			
α-Pinene	0.035	-	-	0.172	-
β-Pinene	0.049	-	-	0.396	-
Pinenes	0.055	-	-	0.299	-
		SOA_{M_F} Tracers			
PNA	**0.609**	**0.548**	**0.527**	−0.071	0.132
PA	*0.483*	**0.663**	*0.486*	0.140	0.007
SOA_{M_F} tracers	**0.601**	**0.586**	**0.518**	−0.041	0.144
		SOA_{M_H} Tracers			
MBTCA	**0.898**	0.042	−0.108	0.040	−0.064
HGA	*0.591*	0.335	*0.455*	0.144	−0.089
HDMGA	**0.650**	0.329	*0.436*	0.060	−0.046
SOA_{M_H} tracers	**0.738**	0.311	0.359	−0.015	−0.085
		SOA_C Tracer			
CA	−0.384	0.045	−0.170	0.345	−0.262

[a]Distance between sites.
[b]Bold indicates a significant correlation at $p < 0.01$.
[c]Italic indicates a significant correlation at $p < 0.05$.

the estimated lifetimes of pinenes reacting with O_3 and OH in China's air. The estimated lifetime of α-pinene reacting with ozone (1.91 h) was a little shorter than that of α-pinene reacting with OH (2.65 h).

The annual average of SOA_C tracer CA ranged from 1.72 to 7.72 ng m^{-3} among the 12 sites. Our measurements are consistent with those reported in different regions of China (Table S2). The highest concentration was observed at the WX site in East China, and the lowest level occurred at the DH site in Northwest China (Figure 4). East China exhibited the highest concentrations among the six regions. The CA levels were higher in southern China than northern China ($p < 0.05$; Figure 2).

3.2. Spatial Homogeneity of SOA Tracers and Pinenes

There were at least two sites within each region, except South China. Since the vegetation was similar between the two sites in each region (Table S1 and Figure S3a), we examined the correlations of SOA tracers between the monitoring sites to investigate the spatial homogeneity of these SOA tracers on a regional scale. The paired-site data of pinenes were only available in East China and Northeast China. Table 1 shows the correlation coefficients of the meteorological parameters, pinenes, and SOA tracers between the inland paired sites based on the 1 year data set.

Although the distance between paired sites varied from 280 to 940 km, the meteorological parameters (temperature, relative humidity, and solar radiation) were significantly correlated ($p < 0.05$) within each region, indicating large spatial homogeneity for the meteorological parameters. The poor correlations ($p > 0.05$) of pinenes suggested a lack of spatial homogeneity on a regional scale. A homogeneous distribution of PNA and PA was observed within a geographical scale of ~400 km ($p < 0.05$). The correlation coefficients of the SOA_{M_F} tracers decreased with increasing distance between sites. When the distance between sites exceeded 450 km (the HL-TYU and DH-SPT pairs), the correlations of the SOA_{M_F} tracers became poor ($p > 0.05$). A significant correlation of SOA_{M_H} tracers was only observed between the WX-HF paired sites ($p < 0.01$).

Thus, our results show different behaviors of pinenes and their SOA tracers. As mentioned above, the concentrations of pinenes in the air depend on emission, oxidation, and transport. Because the emission rates of pinenes are driven by temperature and light [*Guenther et al.*, 2012], the large spatial homogeneity of

meteorological parameters implied a synchronous variation in pinene emissions between the paired sites, since the vegetation types were similar between the two sites within a region. However, the oxidation of pinenes in the gas phase is rapid. The lifetimes of pinenes reacting with OH [*Hofzumahaus et al.*, 2009; *Kanaya et al.*, 2009; *Liu et al.*, 2012] and O_3 [*Zhao et al.*, 2016] in the air of China are within 2–3 h, except for β-pinene ozonolysis (Table S3). Pollutant emissions are influenced by local sources and vary from place to place. For instance, the paired sites within each region exhibited a difference in tropospheric NO_2 vertical column densities (http://avdc.gsfc.nasa.gov/; Figure S3b). This implied that oxidation processes of pinenes in the air would significantly change during transport. The average wind speed at the 12 sites was approximately 4 m s^{-1}. Hence, the transport distance of locally emitted pinenes was only ~43 km within their lifetimes. It should be pointed out that VOC samples were collected for over 1 h. Considering the high diurnal variability in pinene levels, the 1 h sampling might lead to poor correlations of pinenes between sites. All these factors explained the lack of regional characteristics of pinenes.

The SOA_{M_F} tracers are formed mainly through the gas-phase Criegee and/or photochemical reactions of pinenes, followed by the gas-to-particle partitioning [*Eddingsaas et al.*, 2012; *Jenkin et al.*, 2000]. The estimated lifetimes of PNA and PA reacting with OH in the gas phase are ~30 h (Table S3). After partitioning into the particle phase, PNA and PA are expected to have lifetimes as long as those of SOA due to dry and wet deposition (3–7 days) [*Shrivastava et al.*, 2015]. Thus, the transport distance of the SOA_{M_F} tracers could at least reach ~430 km within their lifetimes at a wind speed of 4 m s^{-1}. The changes in pollutant sources and emissions during transport could influence oxidation processes of the SOA_{M_F} tracers in the air. Such an impact might be insignificant on a small scale, considering the relatively slow reactions of the SOA_{M_F} tracers in the air. These explained the regional characteristics of the SOA_{M_F} tracers within a reasonable geographical scale (less than 400 km), whereas homogeneity over a large scale might not be expected. Additionally, the observed correlations might be potentially influenced by other monoterpenes, since δ-limonene and other $C_{10}H_{16}$ compounds could also produce these SOA_M tracers.

As a typical SOA_{M_H} tracer, MBTCA can be formed by the further oxidation of PNA and PA in the gas phase. PNA oxidation by OH forms the corresponding alkylperoxy radicals (RO_2). In the presence of nitrogen oxides, the RO_2 radicals predominantly react with NO to form the intermediate alkoxy radicals (RO). The RO radical further undergoes three possible reactions: (a) dissociation into an alkyl radical and a carbonyl compound; (b) isomerization to an alkyl radical and a hydroxyl function via a hydrogen rearrangement, especially a 1,5 H shift; and (c) reaction with oxygen, forming carbonyl components, and HO_2 [*Müller et al.*, 2012]. After undergoing multiple steps of the above reactions, among which PA is also produced as an intermediate, PNA is eventually converted to MBTCA [*Claeys et al.*, 2007; *Szmigielski et al.*, 2007]. Compared with PNA and PA, MBTCA formation is much more complex. The reaction of RO_2 radicals with NO is vital for the formation of RO radicals. NOx is mainly emitted from local combustion sources in China, such as power plants, industry, and transportation [*Zhao et al.*, 2013]. Thus, the formation of RO radicals is highly influenced by local NO emission, which might lead to poor correlations of SOA_{M_H} tracers between sites over a spatial scale greater than 300 km.

The SOA_C tracer CA was not correlated between paired sites within each region (Table 1). Although the β-caryophyllene emission rate is driven by temperature and light [*Hansen and Seufert*, 2003], β-caryophyllene emissions from plants have large species-to-species differences. As reported by *Curtis et al.* [2014], β-caryophyllene was only detected in one of nine urban tree species. Large tree-to-tree variations in sesquiterpene emissions were observed, even from the same species [*Haapanala et al.*, 2009; *Hakola et al.*, 2001]. Moreover, β-caryophyllene oxidation in the gas phase is very rapid, especially with O_3 (lifetime within 1 min; Table S3). Due to the large variation in β-caryophyllene emissions and the rapid oxidation of β-caryophyllene in the gas phase, there was no significant correlation of CA between sites.

3.3. Seasonal Variations of SOA Tracers and Pinenes

As typical BVOCs, monoterpene emission rates that depend on temperature and light [*Guenther et al.*, 2012] are highest in summer. In addition, due to the influence of bud formation and elongation, monoterpene emission rates could be highest in spring [*Kim*, 2001]. Thus, it is expected that high levels of SOA_M tracers and pinenes occurred in the spring and the summer (Figures 1 and 3). The mass fractions of the SOA_{M_F} tracers in the SOA_M tracers decreased during the summer (Figure 1), probably due to strong photochemistry under high temperature and solar radiation.

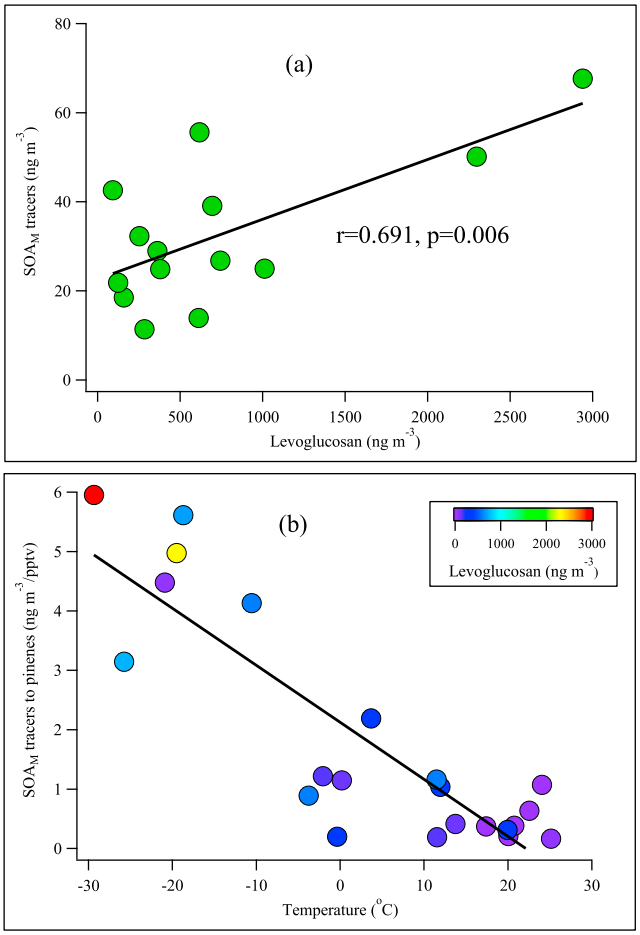

Figure 5. (a) Positive correlation between SOA_M tracers and levoglucosan during the cold period at HL and (b) correlations of the SOA_M tracer to pinene ratios with temperature ($r = -0.865$, $p < 0.001$) and levoglucosan ($r = 0.725$, $p < 0.001$) at HL.

The seasonal variation of SOA_M tracers is also influenced by gas-particle partitioning. As a major SOA_M tracer (average mass fractions of ~50%), PNA was elevated during April and May at most sites (Figure S4). PNA has a subcooled liquid vapor pressure (P_L^0) of 7.8×10^{-4} Pa, with an enthalpy of vaporization (ΔH_{vap}) of 85 kJ mol^{-1} [*Booth et al.*, 2011]. The saturation concentration (C^*) of PNA is estimated as 57 μg m^{-3} by using the gas-particle partitioning model developed by *Donahue et al.* [2006]. The annual average OM ranged from 35 to 86 μg m^{-3} at the 12 sites [*Xin et al.*, 2014]. The resulting calculated particle-phase fractions of PNA in the air of China are within the range of 38%–60% at 298 K. This is consistent with the estimated particle-phase fractions (30–51%; Table S4) based on the group-contribution method [*Donahue et al.*, 2011]. Thus, PNA is highly impacted by gas-particle partitioning. Although high temperature during summer promotes monoterpene emissions, it enhances the gas-phase oxidation of PNA and increases its C^*. The former process reduces the total PNA, and the latter one reduces its particle fractions. This explains why the highest PNA level was not observed during July and August, when temperature was the highest (Figure S4). Unlike PNA, the other four SOA_M tracers all have low volatilities (C^*) and are mainly in the particle phase (Table S4). The sum of the four low-volatile SOA_M tracers exhibited the highest level during July and August at the BJ, TYU, and HF sites (Figure S4).

The concentrations of both semivolatile PNA and the low-volatile SOA_M tracers significantly increased during winter at HL (Figure S4d). The SOA_M tracer levels during winter were higher than those during summer (Figure 1). Due to the defoliation and extremely low temperature in winter (e.g., reaching −29.4°C), biogenic emissions are expected to sharply drop at HL. Thus, there should be sources other than biogenic emissions contributing large amounts of SOA_M during winter at the HL site.

Previous emission inventory studies recorded large amounts of monoterpene emissions from biomass burning (BB), especially from coniferous species [*Akagi et al.*, 2011; *Evtyugina et al.*, 2013; *Lee et al.*, 2005; *Simpson et al.*, 2011; *Yokelson et al.*, 2013]. Monoterpenes can be stored in plant tissue and play defensive roles against insects and pathogens [*Keeling and Bohlmann*, 2006]. As reviewed by *Ciccioli et al.* [2014], vegetation fires not only release substantial amounts of monoterpenes but also influence atmospheric chemistry. In BB plumes, fire-originated monoterpenes dramatically increased O_3 levels [*Akagi et al.*, 2013]. Elevated ambient levels of SOA_M tracers (PNA and PA) were also reported during forest fires [*Yan et al.*, 2008].

Mixed coniferous-broadleaf forest is the dominant forest type in Northeast China [*Dong et al.*, 2014]. During the extremely cold winter, the levels of the BB tracer levoglucosan were as high as 2940 ng m^{-3} at HL and 713 ng m^{-3} at TYU. Negative correlations were observed between levoglucosan and temperature at

Table 2. Correlation Coefficients (r) Between CA and Levoglucosan at Six Sites During Cold Period (Temperature <10°C)

Site	r	p-value
HL	0.804	0.001
TYU	0.582	0.023
BJ	0.581	0.048
SPT	0.664	0.026
QYZ	0.945	0.004
HF	0.833	0.020

HL and TYU ($p < 0.05$). These results indicate that BB for heating significantly increased in the rural and suburban areas of Northeast China. The HL site witnessed a positive correlation between SOA_M tracers and levoglucosan ($r = 0.691$, $p = 0.006$; Figure 5a) during the cold period (temperature <10°C), demonstrating that the significant increase in SOA_M was highly associated with the enhancement of BB.

Moreover, the ratios of SOA_M tracers to pinenes (both in a same sampling episode) increased with decreasing temperature at HL ($r = -0.865$, $p < 0.001$; Figure 5b). The highest ratio of SOA_M tracers to pinenes during the cold period at HL reached 6.0 ng m^{-3}/pptv and was 1 order of magnitude higher than the average (0.46 ng m^{-3}/pptv) during the warm period (temperature >20°C). The enhancement of the ratio of SOA_M tracers to pinenes during the cold period was also observed at the TYU site in Northeast China ($r = -0.760$, $p = 0.001$; Figure S5b) but did not occur at the other four sites (Figures S5c–S5f). Although the ratio of SOA_M tracers to pinenes is not the classic SOA mass yield, it could be applied to reflect the relative strength of SOA_M formation at a site, assuming that vegetation emissions, pollution sources, and meteorology parameters surrounding a site change regularly. High ratios of SOA_M tracers to pinenes during the cold period at HL suggested elevated SOA_M formation strength during the winter. The ratio of SOA_M tracers to pinenes was positively correlated with levoglucosan at HL ($r = 0.725$, $p < 0.001$; Figure 5b), suggesting that the increase in SOA_M formation strength was associated with BB. Thus, the enhancement of BB during winter in Northeast China could elevate the strength of SOA_M formation and produce large amounts of SOA_M. It should be noted that the ratio of SOA_M tracers to pinenes could not be used to compare the relative strengths of SOA_M formation between sites, due to the observed spatial heterogeneity between SOA_M tracers and pinenes as well as the difference in their lifetimes.

The SOA_C tracer CA increased during winter at most sites (Figure 4). Because CA is predominant in the particle phase (Table S4), its seasonal trend has little impact from temperature-driven gas-particle partitioning. Similar to monoterpenes, sesquiterpenes can be synthesized and stored in plant tissue [*Keeling and Bohlmann*, 2006]. Vegetation fires can influence sesquiterpene emissions and SOA formation [*Ciccioli et al.*, 2014; *Mentel et al.*, 2013]. During the cold period, CA was significantly correlated with levoglucosan at six sites (Table 2). A positive correlation between CA and levoglucosan was also reported in springtime over central China by aircraft measurements, indicating substantial contributions from BB to CA production [*Fu et al.*, 2014].

3.4. Biogenic SOC Estimation

These BSOA tracers were further applied to estimate SOC_M and SOC_C over China by using the SOA-tracer method [*Kleindienst et al.*, 2007]. The researchers performed chamber experiments to obtain the mass fraction of tracers in SOC (f_{SOC}) for individual precursors:

$$f_{SOC} = \frac{\sum_i [\mathrm{tri}]}{[\mathrm{SOC}]}$$

where $\sum_i[\mathrm{tri}]$ is the total concentration of the tracers for a certain precursor and [SOC] is the mass concentration of SOC. With these f_{SOC} values and the measured SOA tracers in ambient air, SOC in the atmosphere from different precursors can be estimated, with the assumption that the tracer-SOC relationship obtained in the chamber air is stable in ambient air [*Kleindienst et al.*, 2007].

The f_{SOC} for SOC_M (0.059 μg μgC^{-1}) was calculated by using the chamber data provided by Kleindienst's group [*Offenberg et al.*, 2007] with the same five SOA_M tracers used in this study. The f_{SOC} for β-caryophyllene was 0.023 ± 0.0046 μg μgC^{-1} using CA for SOC_C estimation [*Kleindienst et al.*, 2007]. The same f_{SOC} and tracers were used to estimate SOC_M and SOC_C in our previous studies in the Tibetan Plateau [*Shen et al.*, 2015] and in summertime over China [*Ding et al.*, 2014]. SOC_I during the same period at the 12 sites was estimated by using the SOA-tracer method in our previous study [*Ding et al.*, 2016]. In the following discussion, we will

include SOC_I to provide a full picture of BSOC (sum of SOC_I, SOC_M, and SOC_C) over China. Previous studies showed that these three precursors were major contributors to BSOC [*Fu et al.*, 2012; *Lewandowski et al.*, 2013]. The uncertainty in the SOA-tracer method is caused by the analysis of organic tracers and the determination of the conversion factors. The errors of the tracer analysis were 22% for the SOA_M tracers, 156% for CA, and 40% for the SOC_I tracers. The uncertainties of f_{SOC} were 48% for monoterpenes, 22% for β-caryophyllene, and 25% for isoprene [*Lewandowski et al.*, 2013]. Considering these factors, the uncertainties of the estimated SOC were calculated through error propagation. The RSDs were 53% for SOC_M, 157% for SOC_C, and 47% for SOC_I. It should be noted that the BSOA tracers reported in this study only represent a few of the compounds produced and do not cover all BVOCs (e.g., sesquiterpenes other than β-caryophyllene, as well as other BVOCs). Moreover, there are still significant uncertainties due to the limited number of identified tracers and chamber parameters as well as the simplification of applying organic tracers and conversion factors to calculate BSOA in ambient samples. Additionally, BSOA from aqueous-phase production could not be captured by the SOA-tracer method. Thus, the current results should underestimate total amount of BSOC in the air of China.

The annual average BSOC was $0.91 \pm 0.41\,\mu gC\,m^{-3}$, with the highest concentration at QYZ ($1.52 \pm 0.83\,\mu gC\,m^{-3}$) and the lowest level at SPT ($0.30 \pm 0.24\,\mu gC\,m^{-3}$). Southwest China exhibited the highest concentrations among the six regions, followed by East China, Northeast China, North China, South China, and Northwest China. Southern China presented higher levels of BSOC than northern China. SOC_M was the major component in BSOC (on average, 50%) and ranged from 0.17 to $0.83\,\mu gC\,m^{-3}$ at the 12 sites. SOC_I and SOC_C at the 12 sites were within the ranges of 0.03–$0.63\,\mu gC\,m^{-3}$ and 0.07–$0.34\,\mu gC\,m^{-3}$, respectively. The annual average contributions to BSOC were 28% from SOC_I and 22% from SOC_C.

Modeling studies have simulated BSOC over China. The annual mean BSOC was estimated to be $0.66\,\mu gC\,m^{-3}$ over China by the Goddard Earth Observing System coupled with the Atmospheric Chemistry model (GEOS-Chem) [*Fu et al.*, 2012]. The BSOA in springtime was simulated to be $0.65\,\mu g\,m^{-3}$ over China by the Regional Air Quality Model System (RAQMS) [*Han et al.*, 2016]. The annual average BSOA over China was predicted to be $0.99\,\mu g\,m^{-3}$ by the Weather Research and Forecasting Atmospheric Chemistry model (WRF-Chem) [*Jiang et al.*, 2012]. The SOA-to-SOC ratios in chamber-produced samples were 2.47 ± 0.55, 2.11 ± 0.65, and 1.37 ± 0.15 for SOA_I, SOA_C, and SOA_M, respectively [*Kleindienst et al.*, 2007]. Converting individual SOA to SOC, the model-simulated BSOC over China was $0.40\,\mu gC\,m^{-3}$ in springtime according to the RAQMS model [*Han et al.*, 2016] and $0.58\,\mu gC\,m^{-3}$ during the whole year according to the WRF-Chem model [*Jiang et al.*, 2012]. All three modeling studies presented higher levels of BSOC in southern China than northern China. The model-simulated BSOC levels and spatial distribution are consistent with our ground-based observation.

Figure 6 presents the monthly variation in BSOC at the 12 sites. Generally, high levels of BSOC existed from April to September, and low concentrations occurred during January and February. Significant enhancement of SOC_I was observed from May to September, with SOC_I levels and contributions up to $1.43\,\mu gC\,m^{-3}$ (September at QYZ) and 70% (July at HL), respectively. During October to April, when SOC_I levels dropped, SOC_M composed the majority in BSOC (e.g., 86% in November at QYZ). SOC_C levels significantly increased from November to January.

Figure 7 compares BSOC composition over China between our observation and model simulations. Our 1 year observation at the 12 sites illustrated a majority of SOC_M, followed by SOC_I and SOC_C. For the modeling results, the RAQMS [*Han et al.*, 2016] and WRF-Chem [*Jiang et al.*, 2012] models exhibited a majority of SOC_M. The GEOS-Chem model showed that SOC_I was dominant over SOC_M [*Fu et al.*, 2012], and the SOC_I level agreed with our observation within the uncertainties. As explained by the authors, the discrepancy of the relative abundances of SOC_I and SOC_M in the GEOS-Chem and RAQMS models was because they used larger isoprene emissions and included an additional formation pathway via aqueous chemistry for isoprene [*Fu et al.*, 2012]. It is worth noting that these model results underestimated SOC from sesquiterpenes compared with our observation (Figure 7), although only SOC_C was considered in our study.

Close inspection of our data shows that the BSOC composition changed from season to season, although these changes were not significant relative to the uncertainties (Figure S6). From fall to spring, SOC_M was the majority, and the relative abundances of SOC_I and SOC_C were reversed. The most significant change

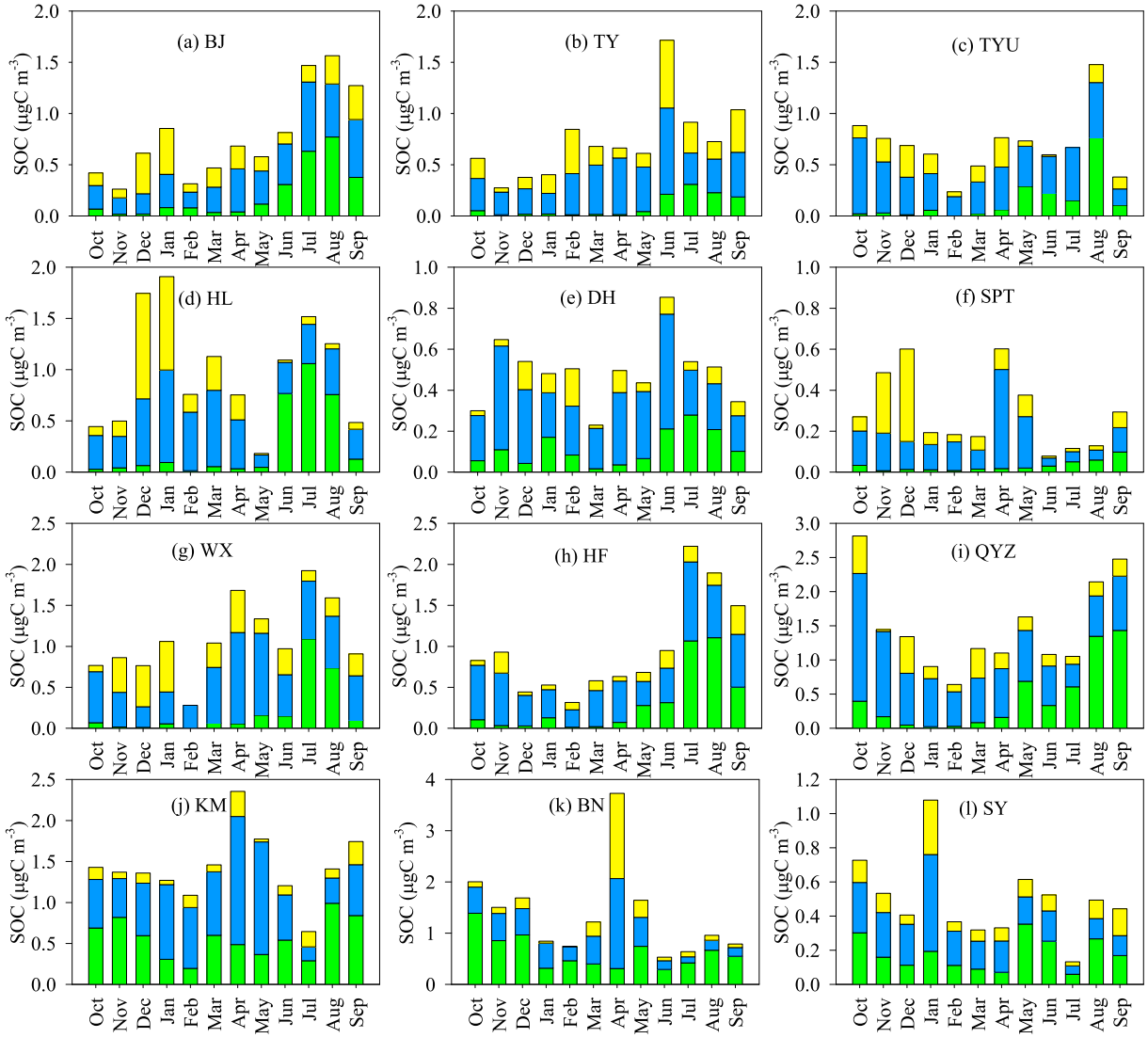

Figure 6. Monthly variation of BSOC at the 12 sites over China. The green, blue, and yellow bars indicate SOC_I, SOC_M, and SOC_C, respectively.

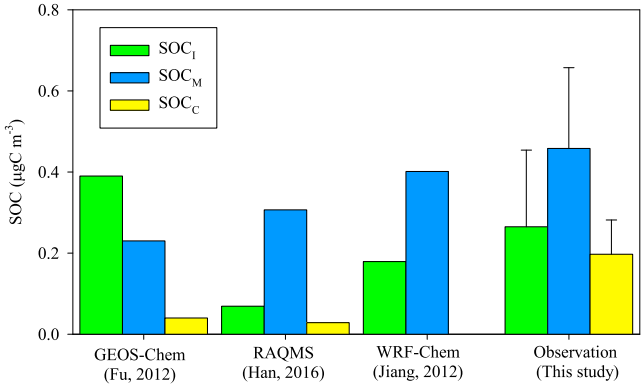

Figure 7. Comparison of BSOC composition over China between model simulation and field observation. The GEOS-Chem and WRF-Chem models estimated annual averages in 2006. The RAQMS model predicted the springtime average in 2009.

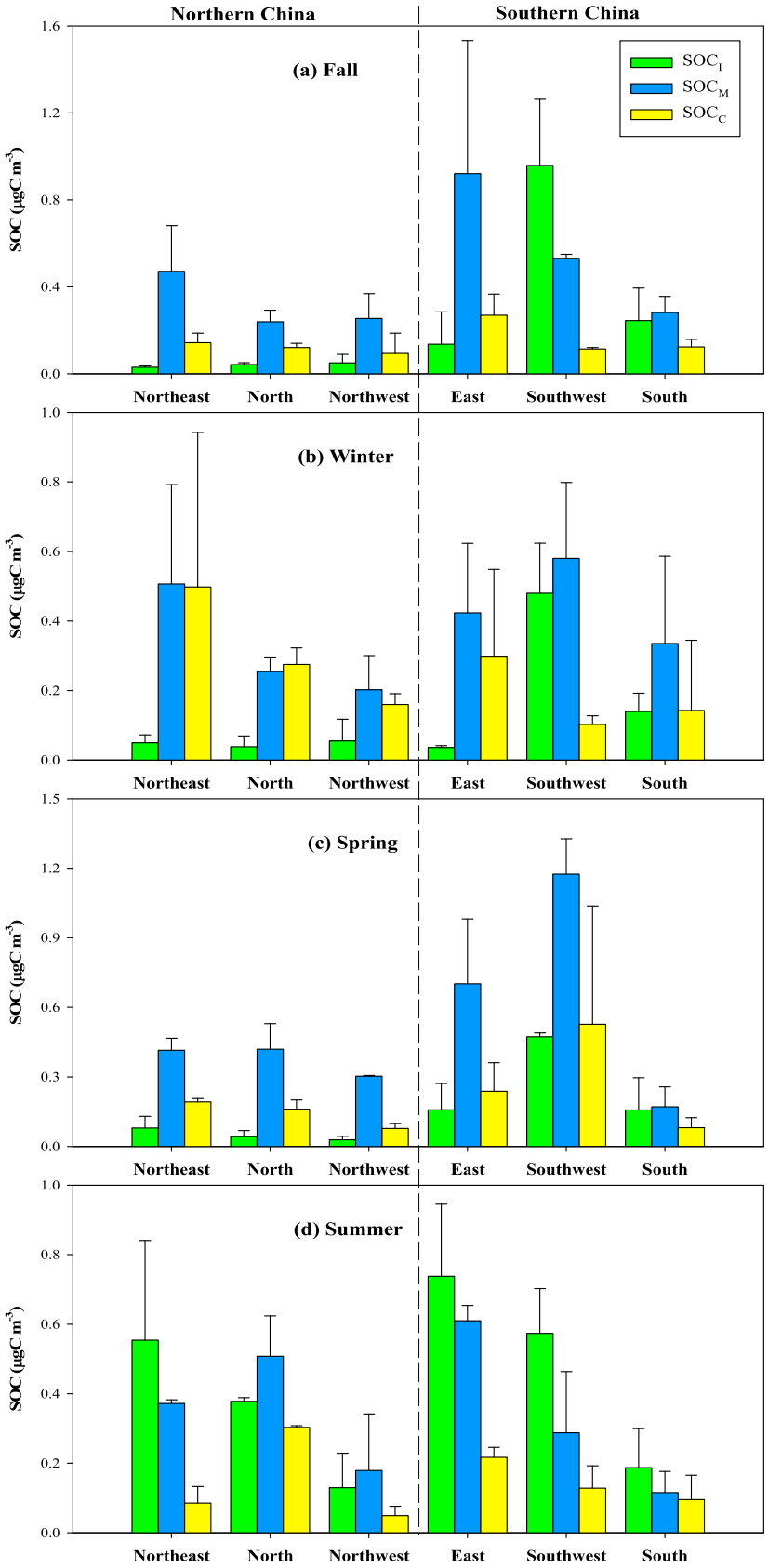

Figure 8. (a–d) Seasonal variation of BSOC in the six regions of China.

was observed during summer, when SOC_I was dominant over SOC_M and SOC_C. This is consistent with our previous observation in summertime at 14 sites across China [*Ding et al.*, 2014]. However, the RAQMS [*Han et al.*, 2008] and WRF-Chem [*Jiang et al.*, 2012] models showed an SOC_M majority during summer. Only the GEOS-Chem model presented an SOC_I majority during summer [*Fu et al.*, 2012].

Figures 8 and S7 present seasonal changes of BSOC composition in the six regions of China. During the fall, SOC_I was the major contributor at KM and BN in Southwest China (Figure S7a), while SOC_M composed the majority in the other five regions (Figure 8a). SOC_C significantly increased during the winter, especially in northern China (Figure 8b). At the HL, BJ, SPT, and WX sites, SOC_C exceeded SOC_M and became the major contributor to BSOC during winter (Figure S7b). During spring, an SOC_M majority was observed at all sites across the six regions (Figures 8c and S7c). SOC_C exceeded SOC_I during fall to spring at all sites in northern China (Figures S7a–S7c). During summer, southern China exhibited a majority of SOC_I (Figure 8d), while northern China exhibited a majority of SOC_M, except at the HL site (Figure S7d).

4. Conclusions

In this study, 1 year ground-based measurements of BSOA tracers and pinenes were undertaken at multiple regions in China. BSOA tracers exhibited higher levels in southern China than northern China. As determined by the ratios of SOA_M tracers ((PNA + PA)/MBTCA, HGA/MBTCA, and PNA/PA), the SOA_M in China was generally SOA_{M_F}, and α-pinene ozonolysis played an important role in SOA_M formation. Pinene, SOA_{M_F}, and SOA_{M_H} tracers showed different regional behaviors. The poor correlations of pinenes between inland paired sites were due to rapid oxidation of pinenes in the air, while the significant correlations of SOA_M tracers between monitoring sites suggested the regional impact of SOA_M. SOA_{M_F} tracers had larger spatial homogeneity than SOA_{M_H} tracers. High levels of SOA_M tracers occurred during spring to summer in China. At HL in Northeast China, however, the concentrations of SOA_M tracers increased during winter. The positive correlation between SOA_M tracers and levoglucosan at HL indicated that the unexpected increase in SOA_M amount was associated with the enhancement of BB during winter. CA significantly increased during winter and was positively correlated with levoglucosan, suggesting substantial contributions from BB to SOA_C production during winter in China. The annual average BSOC was estimated to be $0.91 \pm 0.41\ \mu gC\ m^{-3}$ over China, with the majority from SOC_M and the highest level in Southwest China. High levels of BSOC existed from April to September, and low concentrations occurred in January and February. BSOC composition varied from an SOC_M majority in fall-spring to an SOC_I majority in summer.

China is now suffering from serious PM pollution and visibility reduction. SOA plays an important role during severe haze pollution in China. Our ground-based observation provides detailed information about the characterization of BSOA from monoterpenes and β-caryophyllene, regional differences among northern and southern China, and BB influences on BSOA during winter. In addition, our results illustrate that current model simulations that play important roles in air pollution control in China could not fully capture the seasonal variation in BSOC composition. All these findings are essential to comprehensively understand the sources of China's severe PM problem and to provide guidance for steps to reduce PM levels, particularly during fall to winter, when major incidents have been reported.

Acknowledgments
This research was supported by the Strategic Priority Research Program of the Chinese Academy of Sciences (CAS) (XDA05100104/XDB05010200), the National Science Foundation of China (41530641/41571130031/41473099/41273116), the "Outstanding Young Scientist Project" of the Youth Innovation Promotion Association, CAS, and the State Key Laboratory of Organic Geochemistry (OGL-201213). All SOA tracer, estimated SOC, and pinene data can be found in the supporting information.

References

Akagi, S. K., R. J. Yokelson, C. Wiedinmyer, M. J. Alvarado, J. S. Reid, T. Karl, J. D. Crounse, and P. O. Wennberg (2011), Emission factors for open and domestic biomass burning for use in atmospheric models, *Atmos. Chem. Phys.*, *11*(9), 4039–4072.

Akagi, S. K., et al. (2013), Measurements of reactive trace gases and variable O_3 formation rates in some South Carolina biomass burning plumes, *Atmos. Chem. Phys.*, *13*(3), 1141–1165.

Booth, A. M., W. J. Montague, M. H. Barley, D. O. Topping, G. McFiggans, A. Garforth, and C. J. Percival (2011), Solid state and sub-cooled liquid vapour pressures of cyclic aliphatic dicarboxylic acids, *Atmos. Chem. Phys.*, *11*(2), 655–665.

Ciccioli, P., M. Centritto, and F. Loreto (2014), Biogenic volatile organic compound emissions from vegetation fires, *Plant Cell Environ.*, *37*(8), 1810–1825.

Claeys, M., et al. (2007), Hydroxydicarboxylic acids: Markers for secondary organic aerosol from the photooxidation of α-pinene, *Environ. Sci. Technol.*, *41*(5), 1628–1634.

Curtis, A. J., D. Helmig, C. Baroch, R. Daly, and S. Davis (2014), Biogenic volatile organic compound emissions from nine tree species used in an urban tree-planting program, *Atmos. Environ.*, *95*, 634–643.

de Gouw, J. A., et al. (2008), Sources of particulate matter in the northeastern United States in summer: 1. Direct emissions and secondary formation of organic matter in urban plumes, *J. Geophys. Res.*, *113*, D08301, doi:10.1029/2007JD009243.

Ding, X., M. Zheng, L. Yu, X. Zhang, R. J. Weber, B. Yan, A. G. Russell, E. S. Edgerton, and X. Wang (2008), Spatial and seasonal trends in biogenic secondary organic aerosol tracers and water-soluble organic carbon in the southeastern United States, *Environ. Sci. Technol.*, *42*(14), 5171–5176.

Ding, X., X. Wang, and M. Zheng (2011), The influence of temperature and aerosol acidity on biogenic secondary organic aerosol tracers: Observations at a rural site in the central Pearl River Delta region, South China, *Atmos. Environ.*, *45*(6), 1303–1311.

Ding, X., X. Wang, B. Gao, X. Fu, Q. He, X. Zhao, J. Yu, and M. Zheng (2012), Tracer based estimation of secondary organic carbon in the Pearl River Delta, South China, *J. Geophys. Res.*, *117*, D05313, doi:10.1029/2011JD016596.

Ding, X., X. Wang, Z. Xie, Z. Zhang, and L. Sun (2013), Impacts of Siberian biomass burning on organic aerosols over the North Pacific Ocean and the Arctic: Primary and secondary organic tracers, *Environ. Sci. Technol.*, *47*(7), 3149–3157.

Ding, X., Q.-F. He, R.-Q. Shen, Q.-Q. Yu, and X.-M. Wang (2014), Spatial distributions of secondary organic aerosols from isoprene, monoterpenes, β-caryophyllene, and aromatics over China during summer, *J. Geophys. Res. Atmos.*, *119*, 11,877–11,891, doi:10.1002/2014JD021748.

Ding, X., Q.-F. He, R.-Q. Shen, Q.-Q. Yu, Y.-Q. Zhang, J.-Y. Xin, T.-X. Wen, and X.-M. Wang (2016), Spatial and seasonal variations of isoprene secondary organic aerosol in China: Significant impact of biomass burning during winter, *Sci. Rep.*, *6*, 20411, doi:10.1038/srep20411.

Donahue, N. M., A. L. Robinson, C. O. Stanier, and S. N. Pandis (2006), Coupled partitioning, dilution, and chemical aging of semivolatile organics, *Environ. Sci. Technol.*, *40*(8), 2635–2643.

Donahue, N. M., S. A. Epstein, S. N. Pandis, and A. L. Robinson (2011), A two-dimensional volatility basis set: 1. Organic-aerosol mixing thermodynamics, *Atmos. Chem. Phys.*, *11*(7), 3303–3318.

Dong, L.-B., Z.-G. Liu, F.-R. Li, and L. Jiang (2014), Quantitative analysis of forest spatial structure and optimal species composition for the main forest types in Daxing' anling, Northeast China, *For. Res.*, *27*(6), 734–738.

Eddingsaas, N. C., C. L. Loza, L. D. Yee, M. Chan, K. A. Schilling, P. S. Chhabra, J. H. Seinfeld, and P. O. Wennberg (2012), α-Pinene photooxidation under controlled chemical conditions—Part 2: SOA yield and composition in low- and high-NOx environments, *Atmos. Chem. Phys.*, *12*(16), 7413–7427.

Epstein, S. A., S. L. Blair, and S. A. Nizkorodov (2014), Direct photolysis of α-pinene ozonolysis secondary organic aerosol: Effect on particle mass and peroxide content, *Environ. Sci. Technol.*, *48*(19), 11,251–11,258.

Evtyugina, M., A. I. Calvo, T. Nunes, C. Alves, A. P. Fernandes, L. Tarelho, A. Vicente, and C. Pio (2013), VOC emissions of smouldering combustion from Mediterranean wildfires in central Portugal, *Atmos. Environ.*, *64*, 339–348.

Farina, S. C., P. J. Adams, and S. N. Pandis (2010), Modeling global secondary organic aerosol formation and processing with the volatility basis set: Implications for anthropogenic secondary organic aerosol, *J. Geophys. Res.*, *115*, D09202, doi:10.1029/2009JD013046.

Feng, J., M. Li, P. Zhang, S. Gong, M. Zhong, M. Wu, M. Zheng, C. Chen, H. Wang, and S. Lou (2013), Investigation of the sources and seasonal variations of secondary organic aerosols in $PM_{2.5}$ in Shanghai with organic tracers, *Atmos. Environ.*, *79*, 614–622.

Fu, P. Q., K. Kawamura, Y. F. Cheng, S. Hatakeyama, A. Takami, H. Li, and W. Wang (2014), Aircraft measurements of polar organic tracer compounds in tropospheric particles (PM_{10}) over central China, *Atmos. Chem. Phys.*, *14*(8), 4185–4199.

Fu, P., K. Kawamura, and K. Miura (2011), Molecular characterization of marine organic aerosols collected during a round-the-world cruise, *J. Geophys. Res.*, *116*, D13302, doi:10.1029/12011JD015604.

Fu, T. M., et al. (2012), Carbonaceous aerosols in China: Top-down constraints on primary sources and estimation of secondary contribution, *Atmos. Chem. Phys.*, *12*(5), 2725–2746.

Fu, Y., and H. Liao (2014), Impacts of land use and land cover changes on biogenic emissions of volatile organic compounds in China from the late 1980s to the mid-2000s: Implications for tropospheric ozone and secondary organic aerosol, *Tellus B*, *66*, doi:10.3402/tellusb.v66.24987.

Gómez-González, Y., W. Wang, R. Vermeylen, X. Chi, J. Neirynck, I. A. Janssens, W. Maenhaut, and M. Claeys (2012), Chemical characterisation of atmospheric aerosols during a 2007 summer field campaign at Brasschaat, Belgium: Sources and source processes of biogenic secondary organic aerosol, *Atmos. Chem. Phys.*, *12*(1), 125–138.

Guenther, A. B., X. Jiang, C. L. Heald, T. Sakulyanontvittaya, T. Duhl, L. K. Emmons, and X. Wang (2012), The Model of Emissions of Gases and Aerosols from Nature version 2.1 (MEGAN2.1): An extended and updated framework for modeling biogenic emissions, *Geosci. Model Dev.*, *5*(6), 1471–1492.

Guo, S., M. Hu, Q. Guo, X. Zhang, M. Zheng, J. Zheng, C. C. Chang, J. J. Schauer, and R. Zhang (2012), Primary sources and secondary formation of organic aerosols in Beijing, China, *Environ. Sci. Technol.*, *46*(18), 9846–9853.

Guo, S., et al. (2014), Elucidating severe urban haze formation in China, *Proc. Natl. Acad. Sci. U.S.A.*, *111*(49), 17,373–17,378.

Haapanala, S., A. Ekberg, H. Hakola, V. Tarvainen, J. Rinne, H. Hellén, and A. Arneth (2009), Mountain birch—Potentially large source of sesquiterpenes into high latitude atmosphere, *Biogeosciences*, *6*(11), 2709–2718.

Hakola, H., T. Laurila, V. Lindfors, H. Hellen, A. Gaman, and J. Rinne (2001), Variation of the VOC emission rates of birch species during the growing season, *Boreal Environ. Res.*, *6*(3), 237–249.

Hallquist, M., et al. (2009), The formation, properties and impact of secondary organic aerosol: Current and emerging issues, *Atmos. Chem. Phys.*, *9*(14), 5155–5235.

Han, Z. W., R. J. Zhang, Q. G. Wang, W. Wang, J. J. Cao, and J. Xu (2008), Regional modeling of organic aerosols over China in summertime, *J. Geophys. Res.*, *113*, D11202, doi:10.1029/2007JD009436.

Han, Z., Z. Xie, G. Wang, R. Zhang, and J. Tao (2016), Modeling organic aerosols over east China using a volatility basis-set approach with aging mechanism in a regional air quality model, *Atmos. Environ.*, *124*(Part B), 186–198.

Hand, J. L., et al. (2011), Spatial and seasonal patterns and temporal variability of haze and its constituents in the United States, Report V.

Hansen, U., and G. Seufert (2003), Temperature and light dependence of β-caryophyllene emission rates, *J. Geophys. Res.*, *108*(D24), 4801, doi:10.1029/2003JD003853.

Heald, C. L., et al. (2008), Predicted change in global secondary organic aerosol concentrations in response to future climate, emissions, and land use change, *J. Geophys. Res.*, *113*, D05211, doi:10.1029/2007JD009092.

Hofzumahaus, A., et al. (2009), Amplified trace gas removal in the troposphere, *Science*, *324*(5935), 1702–1704.

Hu, D., Q. Bian, T. W. Y. Li, A. K. H. Lau, and J. Z. Yu (2008), Contributions of isoprene, monoterpenes, β-caryophyllene, and toluene to secondary organic aerosols in Hong Kong during the summer of 2006, *J. Geophys. Res.*, *113*, D22206, doi:10.1029/2008JD010437.

Huang, R.-J., et al. (2014), High secondary aerosol contribution to particulate pollution during haze events in China, *Nature*, *514*, 218–222.

Jaoui, M., T. E. Kleindienst, M. Lewandowski, J. H. Offenberg, and E. O. Edney (2005), Identification and quantification of aerosol polar oxygenated compounds bearing carboxylic or hydroxyl groups. 2. Organic tracer compounds from monoterpenes, *Environ. Sci. Technol.*, *39*(15), 5661–5673.

Jenkin, M. E., D. E. Shallcross, and J. N. Harvey (2000), Development and application of a possible mechanism for the generation of cis-pinic acid from the ozonolysis of α- and β-pinene, *Atmos. Environ.*, *34*(18), 2837–2850.

Jiang, F., Q. Liu, X. Huang, T. Wang, B. Zhuang, and M. Xie (2012), Regional modeling of secondary organic aerosol over China using WRF/Chem, *J. Aerosol Sci.*, *43*(1), 57–73.

Kanaya, Y., et al. (2009), Rates and regimes of photochemical ozone production over Central East China in June 2006: A box model analysis using comprehensive measurements of ozone precursors, *Atmos. Chem. Phys.*, *9*(20), 7711–7723.

Keeling, C. I., and J. Bohlmann (2006), Genes, enzymes and chemicals of terpenoid diversity in the constitutive and induced defence of conifers against insects and pathogens, *New Phytol.*, *170*(4), 657–675.

Kim, J.-C. (2001), Factors controlling natural VOC emissions in a southeastern US pine forest, *Atmos. Environ.*, *35*(19), 3279–3292.

Kleindienst, T. E., M. Jaoui, M. Lewandowski, J. H. Offenberg, C. W. Lewis, P. V. Bhave, and E. O. Edney (2007), Estimates of the contributions of biogenic and anthropogenic hydrocarbons to secondary organic aerosol at a southeastern US location, *Atmos. Environ.*, *41*(37), 8288–8300.

Lal, V., A. F. Khalizov, Y. Lin, M. D. Galvan, B. T. Connell, and R. Zhang (2012), Heterogeneous reactions of epoxides in acidic media, *J. Phys. Chem. A*, *116*(24), 6078–6090.

Lee, S., K. Baumann, J. J. Schauer, R. J. Sheesley, L. P. Naeher, S. Meinardi, D. R. Blake, E. S. Edgerton, A. G. Russell, and M. Clements (2005), Gaseous and particulate emissions from prescribed burning in Georgia, *Environ. Sci. Technol.*, *39*(23), 9049–9056.

Lewandowski, M., I. R. Piletic, T. E. Kleindienst, J. H. Offenberg, M. R. Beaver, M. Jaoui, K. S. Docherty, and E. O. Edney (2013), Secondary organic aerosol characterisation at field sites across the United States during the spring–summer period, *Int. J. Environ. Anal. Chem.*, *93*(10), 1084–1103.

Li, J. J., G. H. Wang, X. M. Wang, J. J. Cao, T. Sun, C. L. Cheng, J. J. Meng, T. F. Hu, and S. X. Liu (2013), Abundance, composition and source of atmospheric $PM_{2.5}$ at a remote site in the Tibetan Plateau, China, *Tellus B*, *65*, 20281, doi:10.3402/tellusb.v65i0.20281.

Li, L. Y., and S. D. Xie (2014), Historical variations of biogenic volatile organic compound emission inventories in China, 1981–2003, *Atmos. Environ.*, *95*, 185–196.

Lin, G., J. E. Penner, and C. Zhou (2016), How will SOA change in the future?, *Geophys. Res. Lett.*, *43*, 1718–1726, doi:10.1002/2015GL067137.

Liu, Z., et al. (2012), Summertime photochemistry during CAREBeijing-2007: ROx budgets and O3 formation, *Atmos. Chem. Phys.*, *12*(16), 7737–7752.

Ma, Y., A. T. Russell, and G. Marston (2008), Mechanisms for the formation of secondary organic aerosol components from the gas-phase ozonolysis of alpha-pinene, *Phys. Chem. Chem. Phys.*, *10*(29), 4294–4312.

Mentel, T. F., et al. (2013), Secondary aerosol formation from stress-induced biogenic emissions and possible climate feedbacks, *Atmos. Chem. Phys.*, *13*(17), 8755–8770.

Müller, L., M. C. Reinnig, K. H. Naumann, H. Saathoff, T. F. Mentel, N. M. Donahue, and T. Hoffmann (2012), Formation of 3-methyl-1,2,3-butanetricarboxylic acid via gas phase oxidation of pinonic acid—A mass spectrometric study of SOA aging, *Atmos. Chem. Phys.*, *12*(3), 1483–1496.

Offenberg, J. H., C. W. Lewis, M. Lewandowski, M. Jaoui, T. E. Kleindienst, and E. O. Edney (2007), Contributions of toluene and α-pinene to SOA formed in an irradiated toluene/α-pinene/NO_x/ air mixture: Comparison of results using ^{14}C content and SOA organic tracer methods, *Environ. Sci. Technol.*, *41*(11), 3972–3976.

Presto, A. A., K. E. HuffHartz, and N. M. Donahue (2005), Secondary organic aerosol production from terpene ozonolysis. 1. Effect of UV radiation, *Environ. Sci. Technol.*, *39*(18), 7036–7045.

Pye, H. O. T., A. W. H. Chan, M. P. Barkley, and J. H. Seinfeld (2010), Global modeling of organic aerosol: The importance of reactive nitrogen (NO_x and NO_3), *Atmos. Chem. Phys.*, *10*(22), 11,261–11,276.

Saleh, R., N. M. Donahue, and A. L. Robinson (2013), Time scales for gas-particle partitioning equilibration of secondary organic aerosol formed from alpha-pinene ozonolysis, *Environ. Sci. Technol.*, *47*(11), 5588–5594.

Sheehan, P. E., and F. M. Bowman (2001), Estimated effects of temperature on secondary organic aerosol concentrations, *Environ. Sci. Technol.*, *35*(11), 2129–2135.

Shen, R. Q., X. Ding, Q. F. He, Z. Y. Cong, Q. Q. Yu, and X. M. Wang (2015), Seasonal variation of secondary organic aerosol tracers in Central Tibetan Plateau, *Atmos. Chem. Phys.*, *15*(15), 8781–8793.

Shrivastava, M., et al. (2015), Global transformation and fate of SOA: Implications of low-volatility SOA and gas-phase fragmentation reactions, *J. Geophys. Res. Atmos.*, *120*, 4169–4195, doi:10.1002/2014JD022563.

Simpson, I. J., et al. (2011), Boreal forest fire emissions in fresh Canadian smoke plumes: C_1-C_{10} volatile organic compounds (VOCs), CO_2, CO, NO_2, NO, HCN and CH_3CN, *Atmos. Chem. Phys.*, *11*(13), 6445–6463.

Sindelarova, K., C. Granier, I. Bouarar, A. Guenther, S. Tilmes, T. Stavrakou, J. F. Müller, U. Kuhn, P. Stefani, and W. Knorr (2014), Global data set of biogenic VOC emissions calculated by the MEGAN model over the last 30 years, *Atmos. Chem. Phys.*, *14*(17), 9317–9341.

Song, Y., M. Shao, Y. Liu, S. Lu, W. Kuster, P. Goldan, and S. Xie (2007), Source apportionment of ambient volatile organic compounds in Beijing, *Environ. Sci. Technol.*, *41*(12), 4348–4353.

Sun, Y., Q. Jiang, Z. Wang, P. Fu, J. Li, T. Yang, and Y. Yin (2014), Investigation of the sources and evolution processes of severe haze pollution in Beijing in January 2013, *J. Geophys. Res. Atmos.*, *119*, 4380–4398, doi:10.1002/2014JD021641.

Szmigielski, R., et al. (2007), 3-Methyl-1,2,3-butanetricarboxylic acid: An atmospheric tracer for terpene secondary organic aerosol, *Geophys. Res. Lett.*, *34*, L24811, doi:10.1029/2007GL031338.

Tang, J. H., L. Y. Chan, C. C. Chang, S. Liu, and Y. S. Li (2009), Characteristics and sources of non-methane hydrocarbons in background atmospheres of eastern, southwestern, and southern China, *J. Geophys. Res.*, *114*, D03304, doi:10.1029/2008JD010333.

Tie, X., G. Li, Z. Ying, A. Guenther, and S. Madronich (2006), Biogenic emissions of isoprenoids and NO in China and comparison to anthropogenic emissions, *Sci. Total Environ.*, *371*(1–3), 238–251.

Wang, S., D. Wu, X.-M. Wang, J. C.-H. Fung, and J. Z. Yu (2013), Relative contributions of secondary organic aerosol formation from toluene, xylenes, isoprene, and monoterpenes in Hong Kong and Guangzhou in the Pearl River Delta, China: An emission-based box modeling study, *J. Geophys. Res. Atmos.*, *118*, 507–519, doi:10.1029/2012JD017985.

Xin, J., et al. (2014), The campaign on atmospheric aerosol research network of China: CARE-China, *Bull. Am. Meteorol. Soc.*, *96*(7), 1137–1155.

Yan, B., M. Zheng, Y. T. Hu, S. Lee, H. K. Kim, and A. G. Russell (2008), Organic composition of carbonaceous aerosols in an aged prescribed fire plume, *Atmos. Chem. Phys.*, *8*, 6381–6394.

Yokelson, R. J., et al. (2013), Coupling field and laboratory measurements to estimate the emission factors of identified and unidentified trace gases for prescribed fires, *Atmos. Chem. Phys.*, *13*(1), 89–116.

Zhang, Q., et al. (2007), Ubiquity and dominance of oxygenated species in organic aerosols in anthropogenically-influenced Northern Hemisphere midlatitudes, *Geophys. Res. Lett.*, *34*, L13801, doi:10.1029/2007GL029979.

Zhang, Q., K. He, and H. Huo (2012a), Policy: Cleaning China's air, *Nature*, *484*(7393), 161–162.

Zhang, X., R. C. McVay, D. D. Huang, N. F. Dalleska, B. Aumont, R. C. Flagan, and J. H. Seinfeld (2015a), Formation and evolution of molecular products in α-pinene secondary organic aerosol, *Proc. Natl. Acad. Sci. U.S.A.*, *112*(46), 14,168–14,173.

Zhang, Y., et al. (2012b), Aromatic hydrocarbons as ozone precursors before and after outbreak of the 2008 financial crisis in the Pearl River Delta region, south China, *J. Geophys. Res.*, *117*, D15306, doi:10.1029/2011JD017356.

Zhang, Z., X. Wang, Y. Zhang, S. Lü, Z. Huang, X. Huang, and Y. Wang (2015b), Ambient air benzene at background sites in China's most developed coastal regions: Exposure levels, source implications and health risks, *Sci. Total Environ.*, *511*, 792–800.

Zhao, B., S. X. Wang, H. Liu, J. Y. Xu, K. Fu, Z. Klimont, J. M. Hao, K. B. He, J. Cofala, and M. Amann (2013), NOx emissions in China: Historical trends and future perspectives, *Atmos. Chem. Phys.*, *13*(19), 9869–9897.

Zhao, S., Y. Yu, D. Yin, J. He, N. Liu, J. Qu, and J. Xiao (2016), Annual and diurnal variations of gaseous and particulate pollutants in 31 provincial capital cities based on in situ air quality monitoring data from China National Environmental Monitoring Center, *Environ. Int.*, *86*, 92–106.